10

UA/PHYS/PET/14-7-98
Submitted to IEEE Trans Med Imaging

UA-PHYS-PET-14-7-98

# Design and Performance Evaluation of a New High Resolution Array Module for PET

JUL 22 1998

George Tzanakos[1,2,*] and Sotiris Pavlopoulos[2,†]

[1]University of Athens, Dept. of Physics, Div. Nuclear & Particle Physics, Athens 15771, Greece
[2]Rutgers University, Department of Biomedical Engineering, Piscataway, New Jersey 08855-0909, USA

Fermilab Library
0 1160 0067028 5

***Abstract* - We have designed a 2-D detector-array for high resolution PET scanners. The module consists of a partially segmented BGO block made of 16 x 18 crystals of dimension 3.35 x 3.30 x 30 mm coupled to a square envelope 3" x 3" position-sensitive PMT. The perfor-mance of the detector module was evaluated using a simulation model that we have developed and the design was optimized to provide high resolution, energy and timing characteristics, and ease in the construction. The energy resolution of the module at the photopeak was estimated to be 27%, whereas the timing resolution of a coincident pair of modules was found to be 6.5 ns FWHM. The detector module has been used as a building block for a high resolution small animal positron tomograph.**

## I. INTRODUCTION

The need for high resolution positron emission tomography (PET) scanner designs along with the absence of small sized photomultipliers (or other kinds of small size detectors of scintillating photons) to accommodate compact designs has lead to the use of block detectors [1-4] made of a 2-D array (4 x 8, 6 x 8, 8 x 8) of small BGO detectors coupled to a 2 x 2 array of commercially available photomultiplier tubes. Based on this gamma-ray detector technology several PET scanners are available, e.g. the GE PC-2048 [5], CTI-931 [6], CTI-831 [7] and CTI-953B [8] that provide high resolution and sensitivity PET images. In most designs however, the resolution is not isotropic, the transaxial resolution being about twice as good as the axial one. In addition the best transaxial resolution is about 3.5 mm.

Recently, there has been an increasing demand for PET system specifically designed for animal studies including oxygen and glucose metabolism and blood flow. Due to the small size of structures involved in small animal studies, high spatial resolution is required. Characteristic examples of such systems are the CTI-713 [9], the MRC small animal scanner [10], the Hamamatsu SHR-2000 [11] and SHR-7700 [12], the TOHR animal scanner [13] and the MicroPET [14]. The first two use 6 x 8 BGO detector block coupled to two dual PMTs whereas the others use small BGO array blocks coupled to position-sensitive PMTs.

TABLE I
GENERAL CHARACTERISTICS OF THE R2487 POSITION-SENSITIVE PMT [17]

| | |
|---|---|
| Dimensions (W x H x L) | 76.1 x 76.1 x 55 mm |
| Spectral Response | 300 to 600 nm |
| Wavelength at Max Response | 420 nm |
| Photocathode Material | Bialkali |
| Active Area | 67.5 mm (X) x59.2 mm (Y) |
| Window Thickness | 3.2 mm |
| Index of Refraction at 420 nm | 1500±0.001 |
| Number of Dynode Stages | 12 |
| Number of Anode Wires | 18 (X) + 16 (Y) |
| Quantum Effic. at peak (390 nm) | 23 % |
| Rise Time (10-90%) | 5.5 ns |
| Electron Transit Time | 17 ns |

We have designed a new high-resolution array module for PET to be used for the construction of a small-animal PET scanner. The module is based on a 18 x 16 partially segmented BGO block coupled to a position sensitive PMT. The performance of the module was evaluated and the design was optimized

* Senior member IEEE. E-mail: tzanakos@atlas.cc.gr
† Presently with the Institute of Communication and Computer Systems, National Technical University of Athens, Greece. Member IEEE. e-mail: spav@biomed.ntua.gr

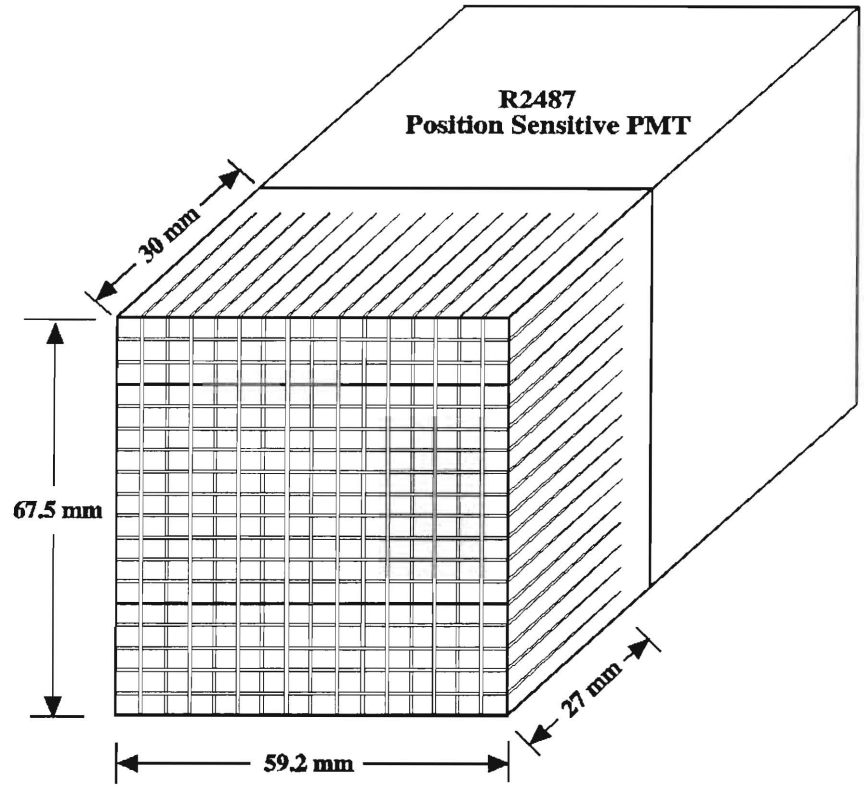


Fig. 1. Schematic representation of the proposed detector module. By cutting horizontal and vertical grooves to a certain depth, a 18 x 16 detector array is formed.

using the Monte Carlo simulation platform that we have developed and validated [15]. It should be noted that this is the first attempt to use simulation techniques to design multicrystal arrays with slotted light guides in the form of horizontal and vertical groves cut into a large scintillator block [16].

## II. Materials and Methods

The proposed detector array module consists of a BGO block forming the detector matrix coupled to a Hamamatsu R2487 position-sensitive PMT[17]. The R2487 is a 3" x 3" square envelope position-sensitive PMT. It has a bialkali photocathode, a 12-stage proximity mesh dynode structure, and multiple anode wires crossing one another in the X and Y directions. The most important characteristics of the PMT tube are summarized in Table I. The cross-wired anodes are spaced by 3.75 mm in the X direction and 3.7 mm in the Y direction. The output signals from each anode are divided trough external resistive chains to produce the X and Y information for the centroid of the illumination of the anode. The spatial resolution of the PMT for 150 incident photons (typical for BGO crystals) is less than 1.5 mm [17], which indicates the possibility to use the particular PMT for high resolution PET scanner designs.

The detector matrix was formed by cutting horizontal and vertical grooves on a single BGO block of 67.5 x 59.2 mm, selected to fully cover the active area of the PMT. To match the number of anode segments of the PMT (18 + 16) 18 horizontal and 16 vertical grooves were cut on the detector block resulting to a total of 288 detectors coupled to a single PMT. The dimensions of each crystal in the array matrix is 3.75 mm x 3.70 mm (W x H). A schematic representation of the proposed detector module is shown in Fig. 1. The advantage of this design is that the array is formed on a single BGO block of 67.5 x 59.2 mm dimensions, even though the individual 3.75 x 3.7 mm detectors are still present. A possible disadvantage of this design would be the increased positioning inaccuracy of the block as a result of the optical crosstalk between individual detectors at the regions where no grooves are present.

To aid the design and the performance evaluation of the proposed detector module we used Monte Carlo simulation techniques. In particular, we used

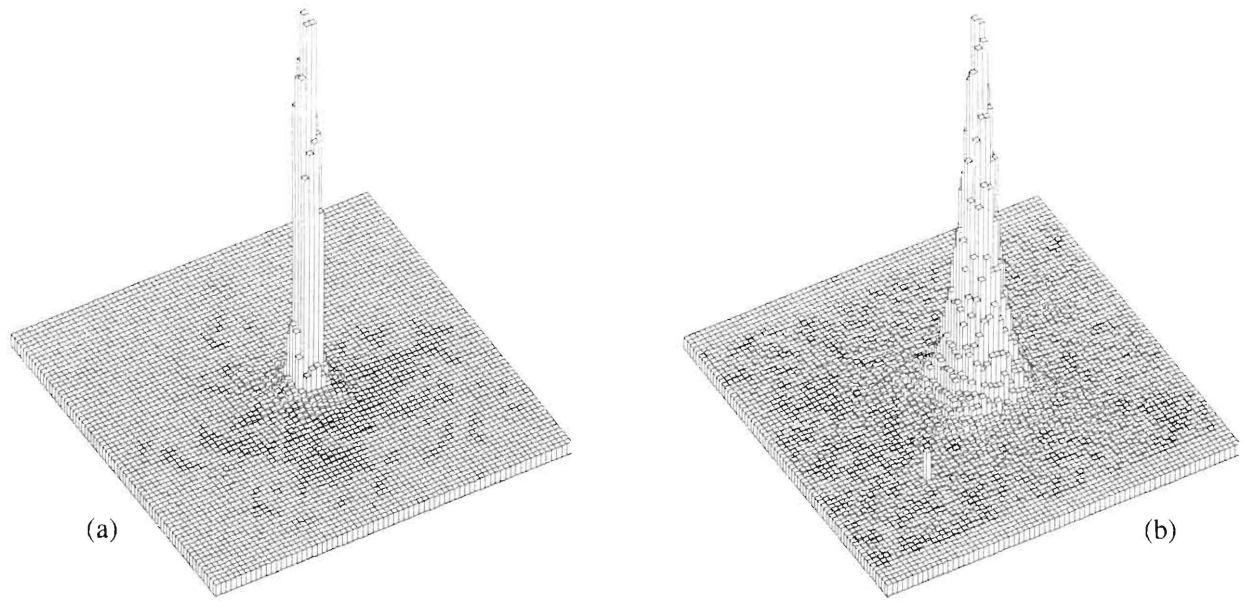


Fig. 2: Distribution of photons arriving at the anode of the PMT when a central region of the detector array was illuminated. The two plots correspond for the case of grooves cut at 30 mm depth (a), and for grooves cut at 27 mm depth (b) respectively.

the simulation model that we have developed and validated for the design of PET scanners [15], [18]-[22]. The model takes into account all physical processes governing -ray propagation and detection, scintillation light generation and propagation, photomultiplier characteristics, and coincidence detection. More details regarding the simulation model can be found in [20]. The design and the performance evaluation of the proposed detector module using simulation techniques are presented in the following section.

## III. Design Considerations - Results

We used our simulation model to study the performance of the proposed BGO block coupled to a single position-sensitive PMT tube (R2487). The length of the BGO block used was 30 mm to ensure the absorption of the majority of incident -rays. As mentioned earlier, the detector matrix is formed by cutting horizontal and vertical grooves along the detector block. Since the depth of the grooves has an important effect in the performance of the detector module, we initially studied the relationship between the depth of the grooves and the positioning accuracy.

The detector matrix was uniformly illuminated with 511 keV -rays propagated inside the detector module. The resulting scintillation photons were propagated inside the detector matrix until they reached to the face of the crystal coupled to the PMT. For every incident -ray, the scintillation photons reaching the photomultiplier window are used to form the energy and timing signals of the PMT. It can be easily understood that for grooves of different length cut along the detector, the distribution of photoelectrons reaching the photocathode of the PMT would differ.

The distributions of photons reaching the photocathode of the PMT when a central region of the detector matrix is illuminated are shown in Fig. 2. The two distributions correspond to the case where the grooves are cut through (30mm depth, which corresponds to the case of individual detectors) and where the grooves are cut at 27mm depth respectively. It is clear that there is an increased spread in the photon distribution as the depth of the grooves is decreased. This is expected to decrease the positioning accuracy of the detector array block.

The main advantage of position-sensitive PMTs is that through their crossed wire anodes they provide information on the X and Y distribution of photons. In particular, each wire provides information on the total number of photons incident on the particular anode region covered by that wire. If $I(x,y)$ is the spatial distribution of photons as they reach to the PMT anode, then we calculate

$$f(x) = \int I(x,y)dy \qquad (1)$$

and

$$g(y) = \int I(x,y)dx \qquad (2)$$

where *f(x) and g(y)* are the crossed wire anode signals. Fig. 3 shows the X crossed wire distribution when a central region of the detector block is illuminated for grooves cut at different depths. It is clear that the deeper the groove is cut the narrower the distribution of photons is within the crossed wires and the more accurate the positioning of the detected -rays will be.

The crossed wire anodes can be connected to resistive chains so that they provide the X and Y coordinates of the centroid of the anode illumination. This can be useful in application where the complexity of the electronics circuitry need to be minimized. The above were simulated in our model by calculating the distribution of photons in both X and Y directions and then estimating the average X and Y position of these distributions. After the X and Y information has been estimated, the positioning accuracy of the design was also estimated by calculating the signed difference between the coordinates of the incident -ray and the estimated coordinates. The spread of the distribution of these differences can be used to quantify the positioning accuracy. This positioning accuracy of the detector array was studied with grooves cut at variable depths and the detector being uniformly illuminated with 511-keV -rays. Fig. 4 shows the distribution of the residuals in the horizontal direction for different depths of the grooves. We can easily see that the deeper the groove is cut, the narrower the spread of the residuals distribution is. In order to quantify the positioning accuracy for different groove depths, the displacement distributions similar to those shown in Fig. 4 were fitted with Gaussian distributions, and the standard deviation of the fitted curves were used as a figure of merit for the positioning accuracy of the detector block. The results of this study are shown in Fig. 5. It is clear from that the highest positioning accuracy is achieved when the grooves are cut through (30 mm depth, which corresponds to the case of individual detectors). In general, the shorter the grooves are cut, the worse the positioning accuracy becomes.

One would like to achieve the positioning accuracy that individual coupling provides by using a detector array block instead of individual crystals. Along that direction, we concentrated on the case of a detector array with grooves cut at 27 mm depth. This design provides a good compromise, since the positioning accuracy is close to that of the individual crystal coupling, and the grooves are short enough to prevent any possible fracture of individual crystals within the block due to their own weight. As shown in Fig. 5, the standard deviations of the distributions of the displacement in the X and Y directions are 2.77 and 2.34 mm respectively. The main factor responsible for the inaccuracy in the event positioning is the optical crosstalk between adjacent crystals, effect that is reduced by cutting deep grooves within the block.

In an effort to identify other factors responsible for the positioning inaccuracy, we illuminated separately each detector in the array and calculated the positioning accuracy for every individual detector. As a result, detectors in the periphery of the array had an absolute displacement larger than detectors at the central regions of the array. Specifically, the average X and Y displacements were found to be dependent on the corresponding row and column indices of the illuminated detector respectively. Fig. 6 shows the dependence of the positioning accuracy as a function of the row and column index of the illuminated detector within the multicrystal array with grooves cut at 27 mm depth. Examining the results drawn from this study, one can conclude that there is a systematic error in positioning the detected event, and the systematic error is larger in the periphery that the center of the detector matrix. It is therefore easily understood that the systematic error in positioning the event would result in the deterioration of the positioning accuracy of the detector array, if no correction is performed in the positioning signals. Using our simulation model we estimated the systematic errors done in positioning events for each crystal of the block being illuminated, and subsequently corrected the positioning signal for the particular systematic error. We then illuminated the block uniformly with 511-keV -rays and calculated the positioning accuracy after the positioning corrections were applied. Fig. 7 shows the displacement distributions when the detector block was uniformly illuminated and the displacement corrections were applied. For comparison purposes, the original distributions (before any corrections were performed) are superimposed. The resolution expressed as the standard deviation of the displacement distributions is 1.89 and 1.73 mm for the X and Y directions respectively. The corresponding resolution before any corrections were performed were 2.77 and 2.34 mm respectively. As we can see, there is a significant improvement in the performance of the detector block

with grooves at 27 mm depth after the positioning correction is performed, and the positioning accuracy is comparable to the accuracy of the case where crystals are coupled individually to the PMT. Clearly the proposed design meets the design requirements; the simplicity that a multicrystal detector array offers combined with a positioning accuracy comparable to the positioning accuracy of individual detectors.

To complete the performance evaluation of the proposed detector unit design, we studied the energy and timing characteristics of the unit. Fig. 8 shows the energy distribution of the detected -rays for a uniform illumination of the front face of the detector unit with 511-keV -rays. The energy resolution at the photopeak is approximately 27% (FWHM) which is comparable to the energy resolution achieved with individual detector-PMT coupling [20]. The good energy resolution of the block is expected to allow the use of high values for the low energy threshold, and subsequently result in the rejection of a significant number of scattered coincidences when used as the building block of a PET scanner. Another advantage of the particular design is the high detection efficiency. For an energy threshold of 375 keV, we estimated detection efficiency of the detector array unit to be 77%. The high detection efficiency of the unit, even for a high value of the energy threshold, is a combined result of the high stopping power of BGO and the size of the detector block used which allows the incident -rays to deposit most of their energy before exiting the block or being photoelectrically absorbed.

Timing resolution is another characteristic that was studied for the proposed detector unit. The timing resolution for a pair of detector units in coincidence is shown in Fig. 9. The timing resolution expressed in FWHM is calculated to be 6.5 ns. Clearly the timing characteristics of the proposed detector unit design are very good (for a BGO based detector unit) and would allow for a short time coincidence window in the coincidence detection circuitry of a PET scanner, thus reducing the number of random coincidences. A reason for the good timing characteristics of the proposed detector module is the absence of the long tails (Fig. 9) usually present in the coincidence timing distributions of BGO detector units as a result of -rays exiting the detectors with only a small fraction of their energy deposited by means of Compton scattering. The proposed detector module design provides enough scintillating material so that a -ray can deposit a significant fraction of its energy before exiting the unit.

## IV. Discussion

Using our simulation model we designed and studied the performance of a new high resolution detector array module for PET. The design is based on a 67.5mm x 59.2 mm x 30mm BGO block coupled to a position sensitive PMT. Horizontal and vertical grooves of 27mm depth form the 18 x 16 crystal matrix. Systematic errors in positioning incident -rays were estimated and corrected, thus providing with positioning resolutions of 1.89 mm and 1.73 mm respectively for the X and Y directions. The energy and timing resolution properties of the detector module were calculated to be 27% and 6.5 ns respectively. All these suggest that the proposed detector module can be used to built high resolution, multi-layer PET scanners. Based on these detector array, a high-resolution small animal positron tomograph has been designed and its performance has been evaluated [22]. The length of the block will have an effect on the dependence of spatial resolution on radial position inside the FOV. This can in part compensated by reducing the length of the block to say 2 cm for BGO, at the expense of sensitivity. Given that new materials have been developed (like LSO) the block can be used with much shorter lengths while being efficient. The same idea of the block using short crystals of CsI could be used for -cameras. We are currently examining the possibility of designing new detector array units incorporating LSO scintillators and latest PS-PMTs.

## References


[1] H. Murayama, N. Nohara, E. Tanaka, and T. Hayashi, ''A quad BGO detector and its timing and positioning discrimination for positron computed tomography", *Nucl. Instr. Meth.*, vol. 192, pp. 501-511, 1982.

[2] M. E. Casey and R. Nutt, ''A multislice two dimensional BGO detector system for PET", *IEEE Trans. Nucl. Sci.*, vol. NS-33, pp. 460-463, 1986.

[3] W. M. Digby, M. Dahlbom, and E. J. Hoffman, ''Detector, Shielding and Geometric Design Factors for a High-Resolution PET System", *IEEE Trans. Nucl. Sci.*, vol. NS-37, No. 2, pp. 664-670, 1990.

[4] J. G. Rogers, A. J. Taylor, M. F. Rahimi, R. Nutt, M. Andreaco, C. W. Williams, An improved multicrystal 2-D BGO detector for PET", *IEEE Trans. Nucl. Sci.*, NS-39, No. 4, pp. 1063-1068, 1992.

[5] A. C. Evans, C. J. Thomson, S. Marrett, E. Meyer and M. Mazza, ''Performance Evaluation of the PC-2048: A New 15-Slice Encoded-Crystal PET Scanner for Neurological Studies, *IEEE Trans. Med. Imag.*, vol. MI-10, No. 1, pp. 90-98, 1991.

[6] T. J. Spinks, T. Jones, M. C. Gilardi and J. D. Heather, ''Performance characteristics of the latest generation of commercial positron scanner", *IEEE Trans. Nucl. Sci.*, vol. NS-35, pp. 721-725, 1988.

[7] E. J. Hoffman, M. E. Phelps, S. C. Huang et. al, ''A New PET system for high resolution 3-dimensional brain

imaging", *J. Nucl. Med.*, vol. 28, pp. 758-759, 1987.

[8] B. Mazoyer, R. Trebossen, R. Deutch, M. Casey and K. Blohm, ''Physical characteristics of the ECAT 953B/31: A New High Resolution Brain Positron Tomograph", *IEEE Trans. Med. Imag.*, vol. MI-10, No. 4, pp. 499-504, 1991.

[9] D. Cutler, S. R. Cherry, E. J. Hoffman, W. M. Digby, and M. E. Phelps, ''Design Features and Performance of a PET System for Animal Research", *J. Nucl. Med.*, vol. 33, No 4, pp. 595-604, 1992.

[10] S. Rajeswaran, D. L. Bailey, et al., ''2-D and 3-D Imaging of Small Animals and the Human Radial Artery with a High Resolution Detector for PET'', *IEEE Trans. Med. Imag.*, Vol. 11, No. 3, pp. 386-391, 1992.

[11] M. Watanabe, H. Uchida, H. Okada, et al., ''A High Resolution PET for Animal Studies", *IEEE Trans. Med. Imag.*, vol. 11, No 4, pp. 577-580, 1992.

[12] M. Watanabe, H. Okada, K. Shimizu, T. Omura, "A High Resolution Animal PET Scanner Using Compact PS-PMT Detectors," *IEEE Trans. Nucl. Sci.*, vol. 44, No. 3, pp. 1277-1282, 1997.

[13] A. Valda Ochoa, L. Ploux, R. Mastrippolito, Y. Charon, P. Laniece, L. Pinot, L. Valentin, "An Original Emission Tomograph for in Vivo Brain Imaging of Small Animals," *IEEE Trans. Nucl. Sci.*, vol. 44, No. 4, pp. 1533-1537, 1997.

[14] S. R. Cherry, Y. Shao, R.W. Silverman, et. al., "MicroPET, "A High Resolution PET scanner for Imaging Small Animals," *IEEE Trans. Nucl. Sci.*, vol. 44, No. 3, pp. 1161-1166, 1997.

[15] G. Tzanakos, M. Bhatia, and S. Pavlopoulos, ``A Monte Carlo Study of the Timing Resolution of $BaF_2$ for TOF PET," *IEEE Trans. Nucl. Sci.*, NS-37, No. 5, pp. 1599-1604, 1990.

[16] G. Tzanakos and S. Pavlopoulos, "Design and Performance Evaluation of a High Resolution Detector Array Module for PET," *Proceedings of the 1993 IEEE Nuclear Science and Medical Imaging Conference*, San Francisco, CA, 1993.

[17] Hamamatsu Photonics K.K., ``Photomultiplier Tubes," Product catalog, 1990.

[18] S. Pavlopoulos, and G. Tzanakos, ``A simulation study of the design of a PET scanner," *Proceedings of the 12th Annual International Conference of the IEEE/EMBS*, eds. P. Pedersen, and B. Onaral, Philadelphia, PA, pp. 139-140, 1990.

[19] S. Pavlopoulos, and G. Tzanakos, ``Modeling a PET scanner," *Proceedings of the 13th Annual International Conference of the IEEE/EMBS*, eds. J. Nagel, and W. Smith, Orlando, FL, pp.213-214, 1991.

[20] G. Tzanakos, and S. Pavlopoulos, ``Development and validation of a simulation model for the design of a PET scanner," *IEEE Trans. Nucl. Sci.*, Vol. NS-39, No. 4, pp. 1093-1098, 1992.

[21] S. Pavlopoulos, and G. Tzanakos, `` A simulation study of certain performance characteristics of the CTI-931 PET tomograph" *Proceedings of the 18th Northeast Bioengineering Conference*, Kingston, RI, March 1992.

[22] S. Pavlopoulos, G. Tzanakos, "Design and Performance Evaluation of a High-Resolution Small Animal Positron Tomograph," *IEEE Trans. Nucl. Sci.*, vol. 43, No. 6, pp.3249-3255, 1996.

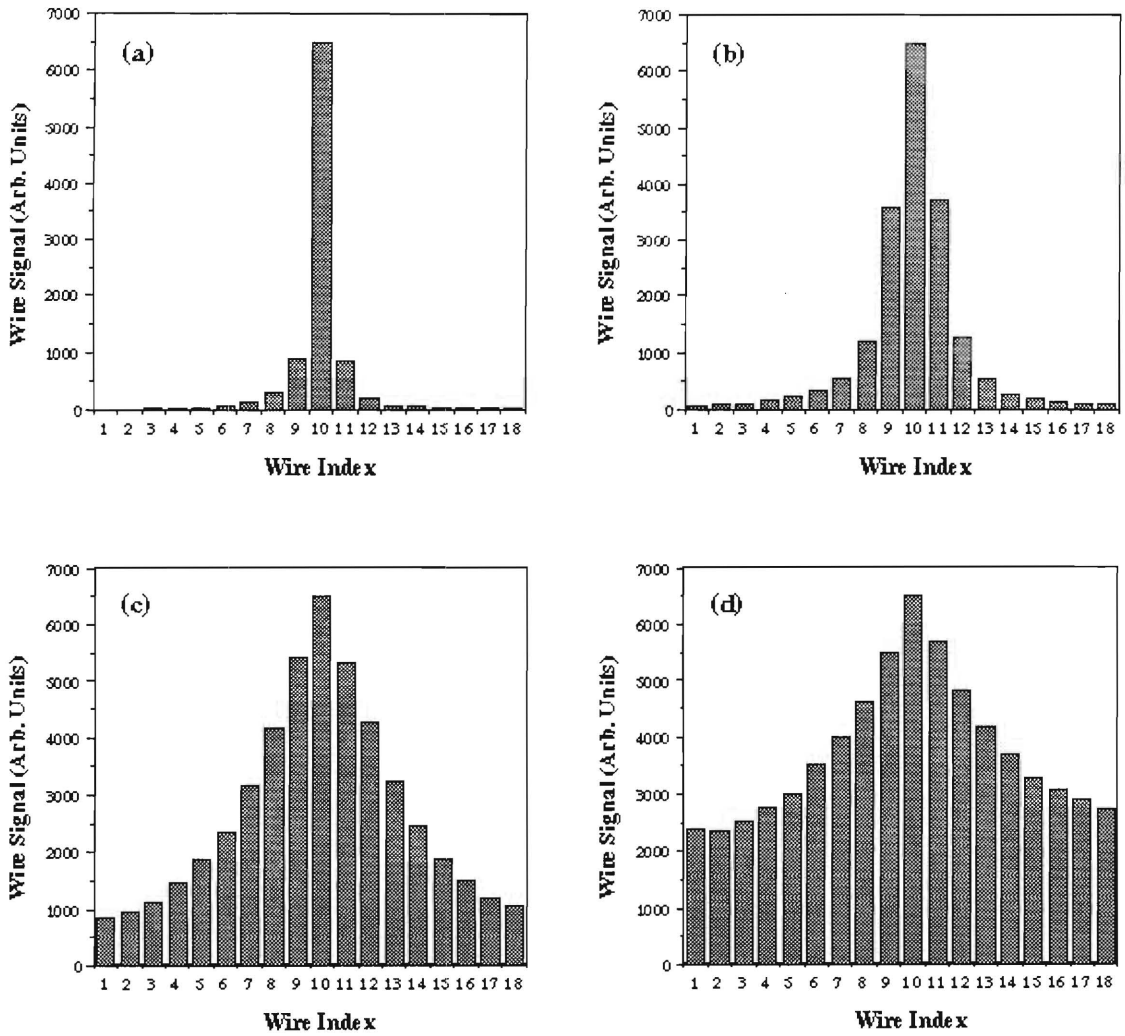


Fig. 3. Distribution of the X crossed wires for illumination of a central region of the detector block with grooves cut 30 mm depth (a), 27 mm depth (b), 18 mm depth (c), and 0 mm depth (d).

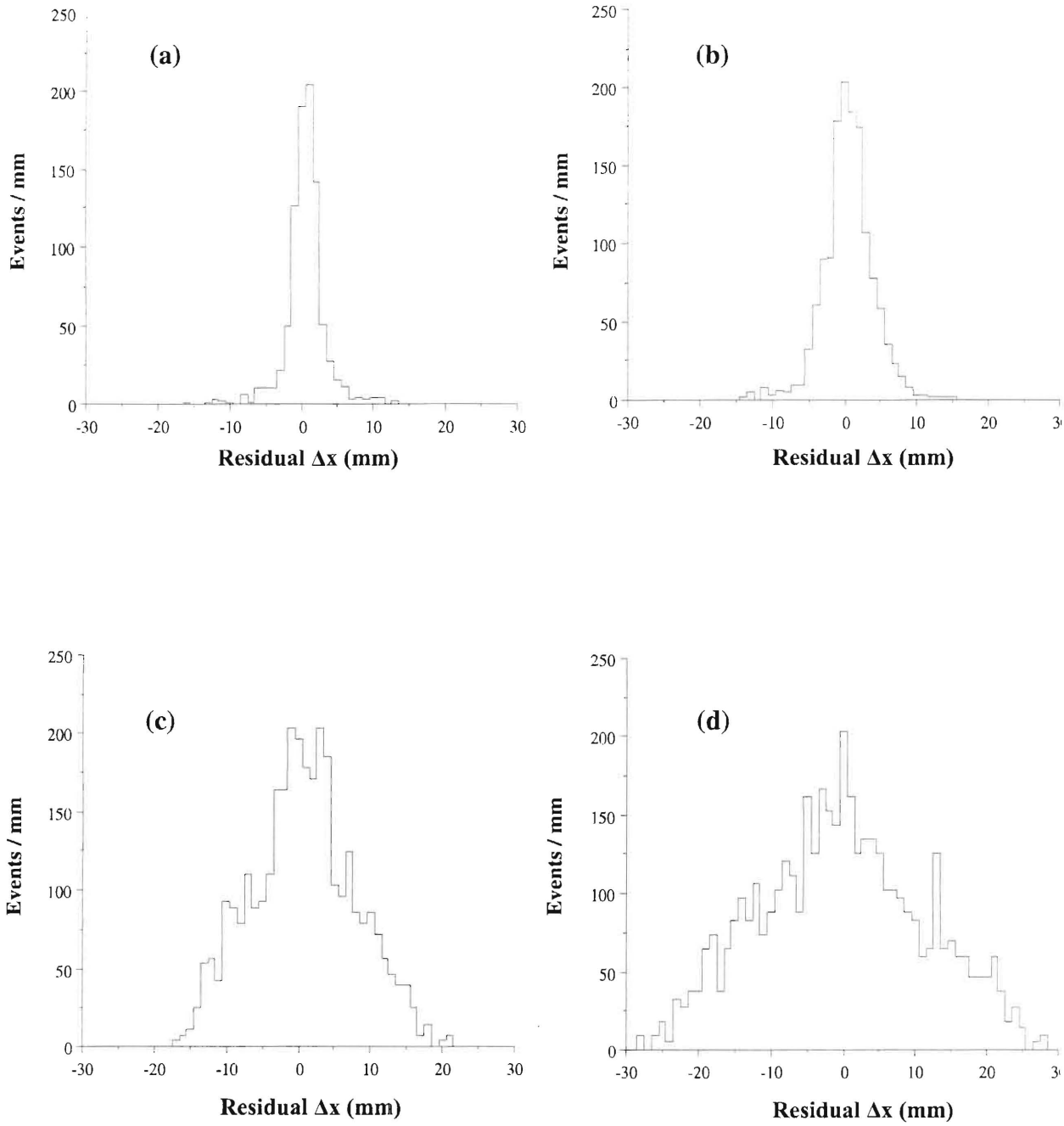


Fig. 4. Horizontal residual x of the detector block with grooves cut30 mm depth (a), 27 mm depth (b), 18 mm depth (c), and 0 mm depth (d). The deeper the grooves, the smaller the residual is.

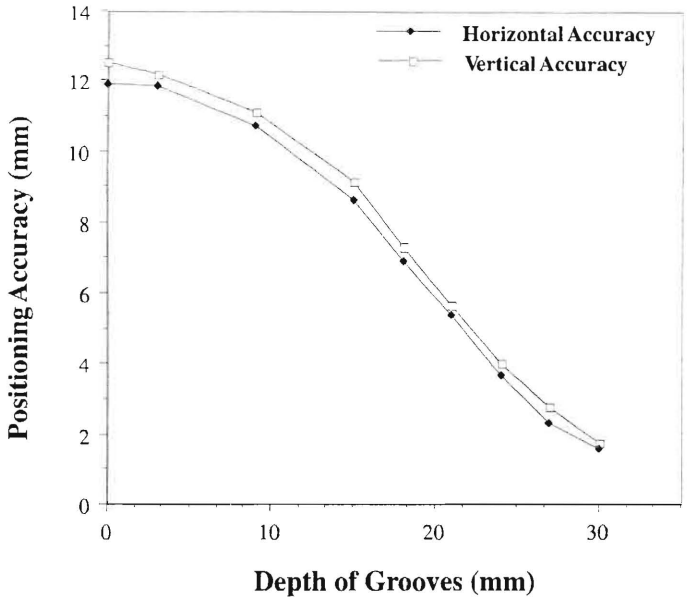


Fig. 5. The positioning accuracy of the detector array is plotted versus the depth of the grooves used. The positioning accuracy was calculated by estimating the standard deviation ( ) of the displacement distribution of the detected -rays.

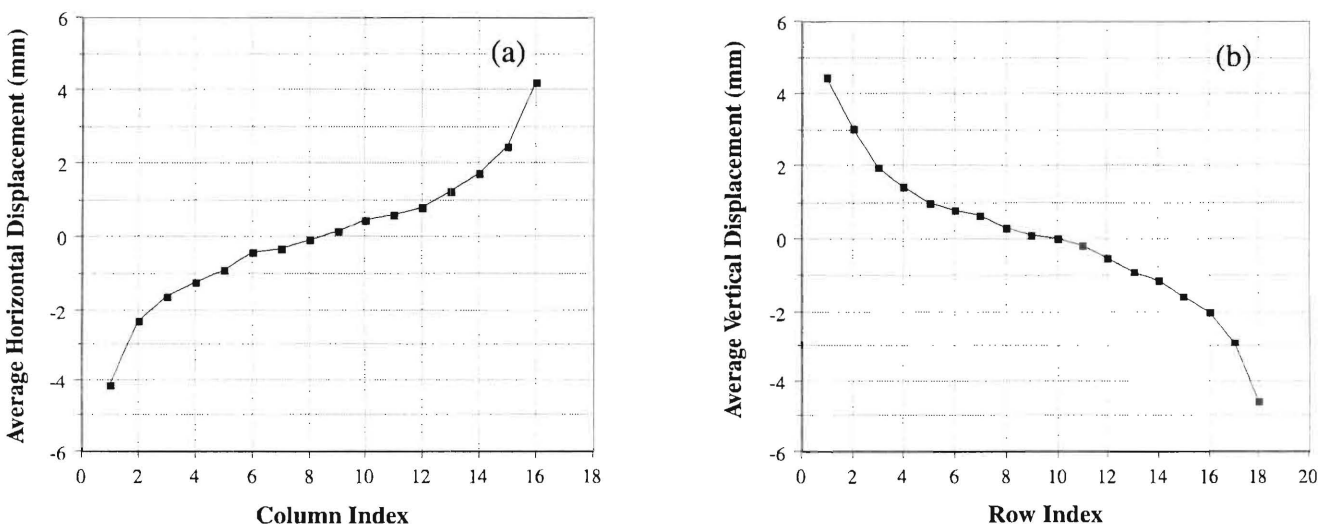


Fig. 6. Average horizontal (a) and vertical (b) displacement dependence with the row and column index of the illuminated detector. Detectors at the center of the block have almost zero average displacements whereas detectors in the periphery have large positive or negative displacements.

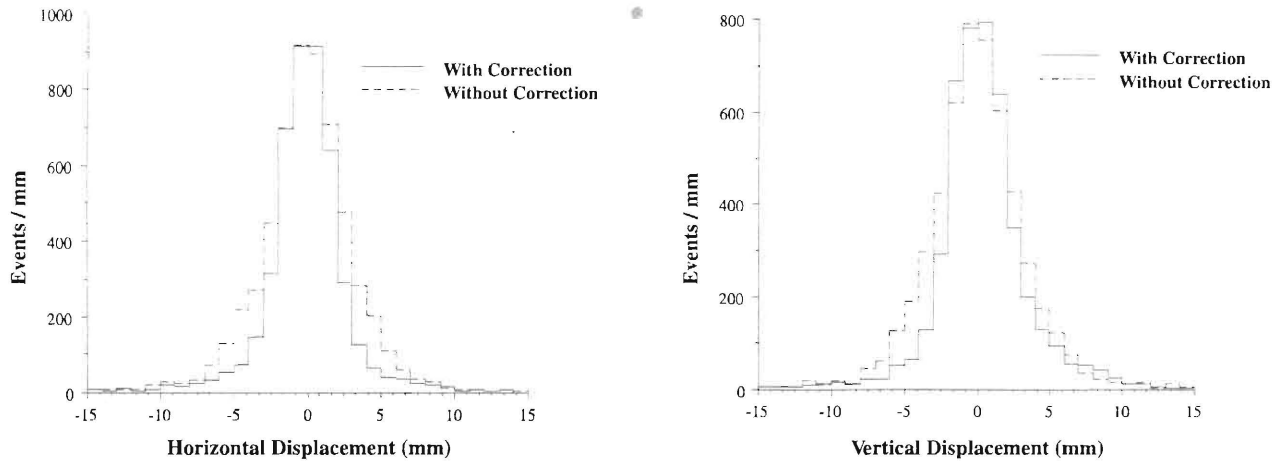


Fig. 7. Positioning accuracy of the detector array with uniform illumination after positioning correction. The accuracy is quantified as the standard deviation of the displacement distributions. Both the horizontal and vertical displacement distributions are shown. For comparison purposes, the correspondent distributions without any corrections are superimposed.

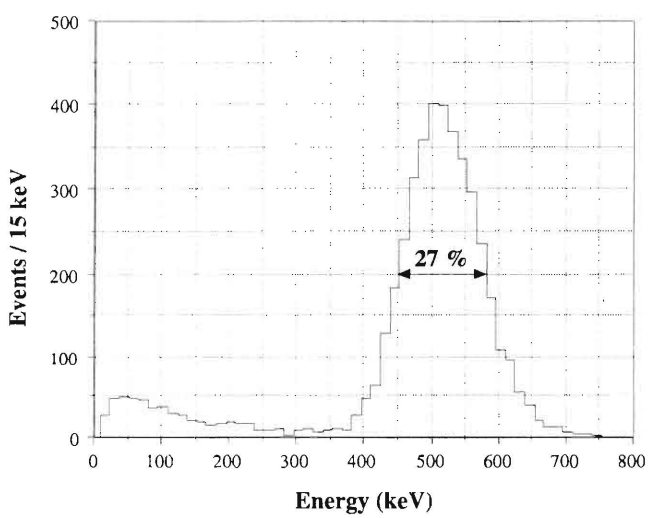


Fig. 8. Energy spectrum of the events detected by the multicrystal detector unit when illuminated uniformly with 511-keV -rays. The resolution at the photopeak expressed in FWHM is 27%.

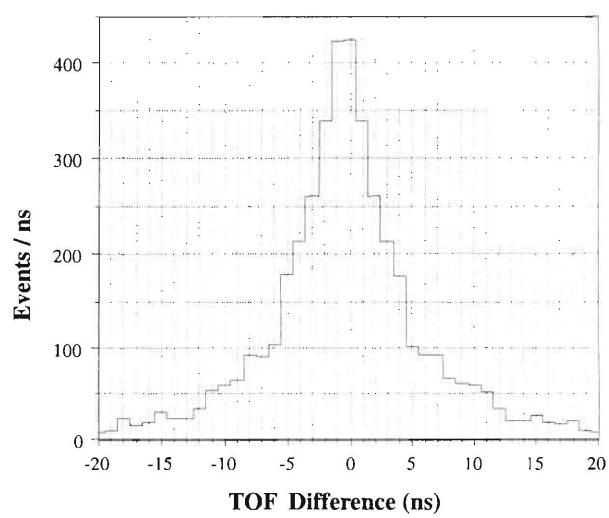


Fig. 9. Distribution of coincident timing signals for a pair of detector units. Timing resolution expressed in FWHM is 6.5 ns.